Functionality and Behaviour of an Dual Kalman Filter implemented on a Modular Battery-Management-System

Conference on Future Automotive Technology: Focus Electromobility

Georg Walder[1], Christian Campestrini[2], Sebastian Kohlmeier[1], Markus Lienkamp[1], Andreas Jossen[2]
[1]*Inst. of Automotive Technology (TU München), Garching, Germany*
[2]*Inst. for Electrical Energy Storage Technology (TU München), Munich, Germany*
E-mail: georg.walder@tum.de

ABSTRACT: Based on the fact that the battery represents the most cost intensive component in a Battery Electric Vehicle (BEV), the usage of the maximum capacity installed is desirable. Therefore, a precise estimation of the State of Charge (SOC) and the State of Health (SOH) is needed, in order to increase the efficiency of the battery. The essential component for estimating the SOC and to supervise the safety is the Battery Management System (BMS). Nowadays, SOC estimation can be done by ampere hour counting, a complex, model-based filter estimation, or others. This paper focuses on the model based filter algorithm. For this analysis, a modular BMS was developed for implementation and verification. This paper presents the combination of the measurement, safety and state estimation components implemented in the software and hardware structure.
The used filter for the state estimation is a Kalman Filter (KF) adapted for the implementation on a BMS. The KF shows a stable behaviour and provides a precise SOC estimation. The selected battery model was a simple electrical equivalent circuit based model that consists of an $R_{DC,1s}$ resistance, a diffusion resistance and a diffusion capacity. Different papers [1] [5] have shown that a model such as the electrical equivalent circuit based model is adequate to provide a precise and fast SOC estimation. To calculate the SOH too, another filter for the battery parameter estimation was added. The resulting Dual Kalman Filter (DKF) combines an effective SOC and SOH estimation. To provide a realistic BEV environment, the battery cells were charged and discharged with the Artemis Driving Cycle via a BaSyTec system.
As the measurement and calculation results presented in the paper show, the KF in combination with the battery model estimates an accurate SOC calculation and the predicted voltage of the KF matches with the real measured battery voltage. A relevant behaviour was the sensitivity of the SOC and SOH estimation related to inaccurate current sensors. The paper reveals that the SOC calculation still has a satisfactory accuracy, while the SOH estimation deviates slowly.

Keywords: Kalman Filter, Dual Kalman Filter, Battery Management System, state estimation, SOC, SOH

1. INTRODUCTION

1.1. BMS Functions

The functionalities of a BMS are divided into in six different categories: The measurement and data processing functions, the safety functions, the balancing function, the power management, the energy management and the thermal management.
The collections of all cell voltages, the readout of the current sensor and the measurement of the temperatures inside the battery pack are the main measurement tasks of the BMS. Dangerous and lifecycle-decreasing states have to be identified and have to be avoided. To detect those operating areas, data processing and data analysing tools are required. To maximize the usable cell capacity and to increase the charging time, an efficient balancing of each cell capacity is desirable. An adequate knowledge of the cell behaviour at different loads results in a useful power prediction and will increase the performance of the entire engine. For a precise range calculation, an interaction between the auxiliary loads, the engine loads and the usable battery capacity is important. To predict different temperature gradients in the battery pack, an adequate detection of the temperature distribution is preferable.
To achieve a reliable range prediction a reliable SOC calculation is implemented. The parameter estimation, like the $R_{DC,1s}$ resistance or the capacity of the cells, is needed to predict the allowed load for each cell. Knowledge of $R_{DC,1s}$ cell losses results in a known temperature behaviour and consequently it is possible to manage the temperatures in the battery pack. Safety issues, such as the detection of cell contacting problems or anticipated cell risks, for example an inner short circuit, could be detected by the BMS as well.

1.2. Methods of SOC calculating

Nowadays several methods of SOC calculations are established. A common method is to integrate the current over time. Equation (1) shows, that in a time-discrete form, the current integration results in a summation of the current at each measurement cycle.

$$SOC(t) = SOC_{t_0=0} - \frac{\int_{t_0}^{t} I(t)dt}{C_N} \xrightarrow[t \to T_s]{} SOC_k = SOC_{k=0} - \frac{\sum_{k=0}^{k} I_k \cdot T_s}{C_N} \quad (1)$$

The accuracy of this method depends on the accuracy of the current sensor used. A sensor drifts and a limited measurement data resolution results in an increasing deviation of the calculated SOC. Calibration options for adapting the calculated SOC to the real SOC are necessary. The calibration could only be done in a load-free mode, when the Open Circuit Voltage (OCV) is measurable at the cell contacts. Typically the calibration of this method is done when the cell is fully charged. When the cell reaches its end of charge voltage, the SOC is set to 100 % after a defined rest time.
Other SOC calculation methods are based on an estimation depending on the terminal voltage of the cell with the actual current. Variations of the $R_{DC,1s}$ resistor and other dynamic procedures result in an increasing error over the cell lifetime.
Several papers [1] [2] describe other SOC calculation methods, based on different Kalman filters. They base on a battery model that describes the static and dynamic behaviour of the battery. Measurable values, such as the current or the terminal cell voltage will be compared to the calculated values of the filter. This error is adapted to the filter parameters and filter states to minimize the error. Compared to other methods, this filter adapts the battery states and parameters over the lifetime.

1.3 Modular BMS

The BMS used for testing the algorithm in a real environment is a self developed system, designed for research institutes and universities. It consists of a modular architecture in which every connection topology is possible. It can be used as a standalone system with only one measurement and one calculation unit or a modular extension with more measurement units and only one calculation unit. A master slave topology is also possible. Figure 1

shows the structure of one BMS unit. The measurement part and the calculating part can be used independently. It is possible to extend six measurement units for only one calculation unit. The following filter design is based on the master slave topology. Because every slave has its own processing unit, the filter is implemented on the slave. The desirable processing power for all cells is therefore partitioned at each slave.

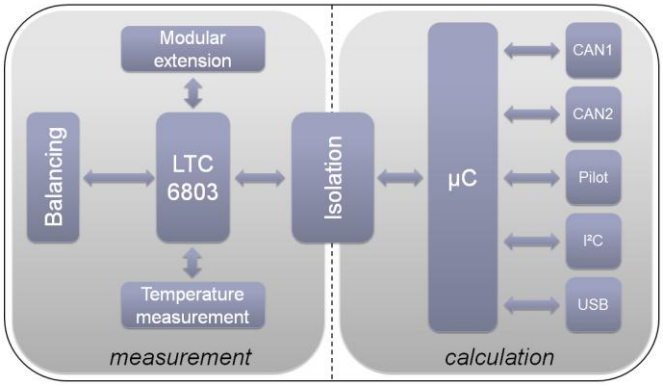

Figure 1: Structure of the used BMS

2. BMS MEASUREMENT AND CALCULATION STRUCTURE

2.1. Measurement Structure

The measurement unit of the used BMS is based on a multi-cell battery stack monitor (LTC6803). It covers the following features: measures up to 12 battery cells in series, on board temperature sensor and thermistor inputs, built-in self-tests, open-wire connection fault detection, delta-sigma converter with built-in noise filter and more. The communication with the external control unit takes place via a 1 MHz serial interface (SPI) with packet error checking. These functions cannot be done simultaneously whereby these measurements and communications have to be subjected to several sequences. Figure 2 shows the sequence for one measurement interval.

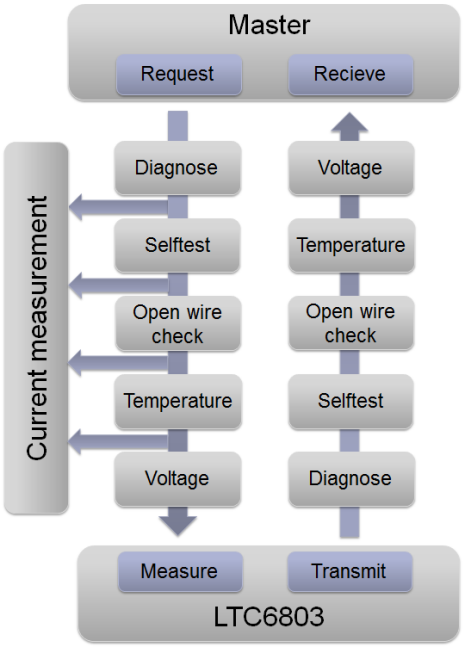

Figure 2: Measurement structure

The measurement classifies into five categories:

1. Cell voltage measurement: measures each cell voltage.
2. Temperature measurement: evaluate the thermistor inputs.
3. Open-wire detection: detects problems in the cell-sensing wires.
4. ADC self-test: checks the functionality of the analogue to digital converter (ADC).
5. Reference voltage diagnosis: checks the functionality of the internal voltage reference.

Because the multi-cell monitor measures successively, the duration of the voltage measurements for 12 cells results in a duration of 50 ms. Based on Figure 2, the voltage sample rate yield is 250 ms. The current will be measured before every measurement command, so the current sample rate is given to 50 ms. Related to Figure 3 in a master slave system the measured values are transmitted to the slave control unit.

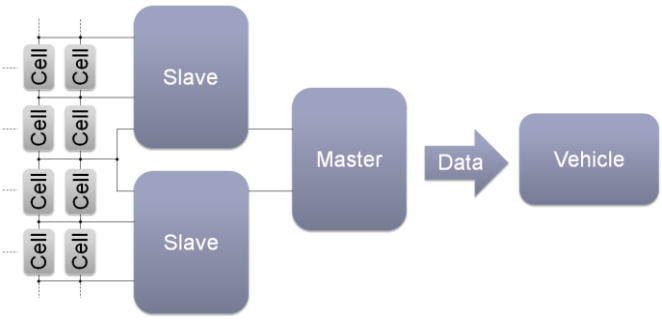

Figure 3: Master slave topology

To demonstrate the differences in the state and parameter estimation, two different current sensors were used. Table 1 shows the accuracy and the measurable range of the current sensors used. The current sensor B was selected to analyse the performance of the KF in order to an inaccurate current sensor.

Table 1: Current sensors used

Sensor	accuracy	range
A: Isabellenhütte IVT-A	±(0.2 % + 30 mA)	±300 A
B: Allegro ACS756	±7. 5 %	±50 A

2.2. Calculation Structure

The slave main task collects the measured data, analyses if there is a safety issue and computes the cell parameter and state calculation of each cell. The converted data will then be transmitted to the master. Each slave consists of a PIC32 (32 Bit) 80 MHz microprocessor with a performance of 125 DMIPS (Dhrystone Million Instructions per second).

For the state and parameter estimation, the voltage and current data have to be referred to the same timestamp, according to the filter calculation interval.

Figure 4 demonstrates the different sequence of the respective measurements and the necessary interpolation to the according calculation timestamp.

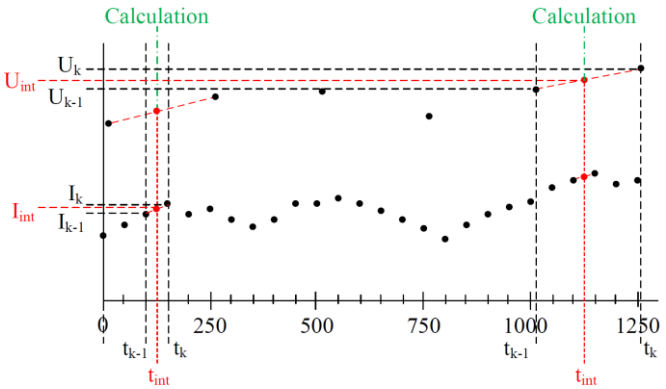

Figure 4: Calculation of the interpolated values

Before the filter algorithm at the BMS starts, the cell voltages were interpolated linearly according to the timestamp of the last measured cell voltage. Equation (2) describes this interpolation procedure:

$$U_{int} = \frac{(U_k - U_{k-1})}{t_k - t_{k-1}} \cdot (t_{int} - t_{k-1}) + U_{k-1} \quad (2)$$

The error of this interpolation depends on the dynamics of the voltage changing between the sample rates.
For the current interpolations, there are two options:

1. Interpolation of the current between the sample points, referred to the necessary calculation timestamp
2. Calculating the mean value of the current between the calculation intervals.

As the next chapter will show, the first option is necessary for an accurate parameter estimation. Equation (3) shows this first option.

$$I_{int} = \frac{(I_k - I_{k-1})}{t_k - t_{k-1}} \cdot (t_{int} - t_{k-1}) + I_{k-1} \quad (3)$$

Equation (4) describes the recursive current mean calculation:

$$I_{mean,k} = \frac{I_{mean,k-1} \cdot (k-1) + I_k}{k} \quad (4)$$

Current variations between the estimation sample time would be unvalued, because only the current value at the proper calculation sample time would influences the used value. The SOC estimator is based on an ampere hour counter and therefore, it will increase the SOC estimation accuracy, if the current value for the SOC calculation part considers the mean value instead the interpolated current. Therefore this second option will improve the filter performance.

3. BATTERY MODEL

To describe the behaviour of a battery, an electrical equivalent circuit is used. The different effects while charging or discharging are modelled with standard electrical parts such as a resistor and capacitor. A previous paper [1] [2]compared different models based on the common Randles equivalent circuit. It was shown that a model with one RC-element (Figure 5) approximates the real behaviour adequately and represents a good conformity between accuracy and computational power for the application in a BMS.

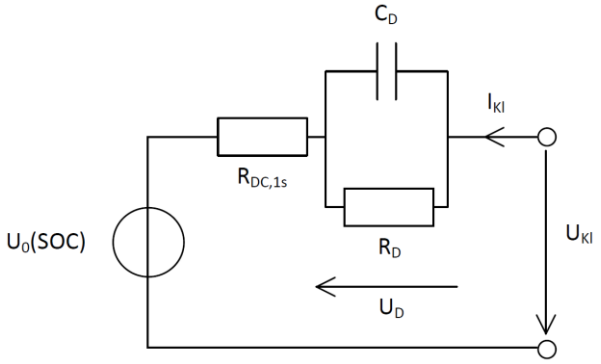

$R_{DC,1s}$ ... resistor calculated 1 s after a current pulse
R_D ... diffusion resistant
C_D ... diffusion capacity
I_{Kl} ... terminal current
U_{Kl} ... terminal voltage
U_D ... diffusion voltage
$U_0(SOC)$ ... SOC depended OCV

Figure 5: A battery modelled by an equivalent circuit

In the model, the terminal voltage consists of the SOC dependent OCV $U_0(SOC)$, the voltage drop over $R_{DC,1s}$ and the diffusion voltage U_D:

$$U_{Kl}(t) = U_0(SOC) + R_{DC,1s} \cdot I_{Kl}(t) + U_D(t) \quad (5)$$

The OCV is related to the proper cell SOC. This correlation is given in Figure 6 and is characteristically for the used cell type. It has to be measured for each cell type individually and reveals one of the most important references to the estimating SOC in the following algorithm.

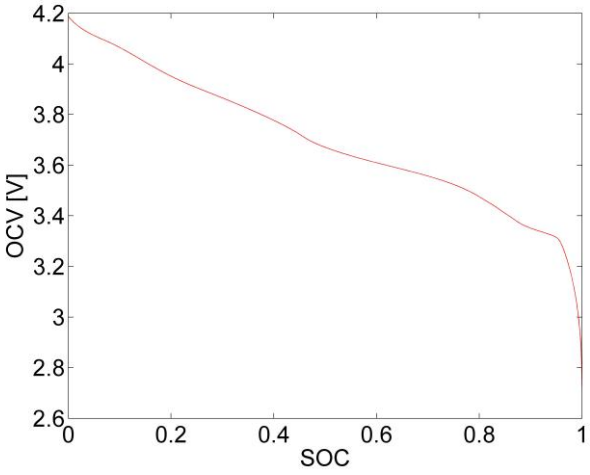

Figure 6: OCV dependency of the SOC

The $R_{DC,1s}$ is the resistor calculated (equation (6)) 1 s after a current pulse and contains the ohmic resistor and parts of the charge transfer resistor.

$$R_{DC,1s} = \frac{\Delta U}{\Delta I} = \frac{U_{t=1s} - U_{t=0}}{I_{t=1s} - I_{t=0}} \quad (6)$$

For the serial resistor the $R_{DC,1s}$ is used, because the calculations for the KF are done every second (Figure 4).
The diffusion voltage $U_D(t)$ is described by a first order differential equation:

$$\dot{U}_D(t) = -\frac{1}{R_D C_D} \cdot U_D(t) + \frac{1}{C_D} \cdot I_{Kl}(t) \quad (7)$$

The state vector $\underline{x}(t) = [x_1, x_2]^T = [U_D(t), SOC(t)]^T$ summarizes the equation as follows:

$$\underline{\dot{x}}(t) = \begin{bmatrix} -\frac{1}{R_D \cdot C_D} & 0 \\ 0 & 0 \end{bmatrix} \underline{x}(t) + \begin{bmatrix} \frac{1}{C_D} \\ \frac{1}{C_N} \end{bmatrix} u(t) \quad (8)$$

$$y(t) = U_0\big(x_2(t)\big) + R_i \cdot u(t) + x_1(t) \quad (9)$$

with the input $u(t) = I_{Kl}(t)$ and the output equation $y(t)$. C_N is the usable capacity of the battery.

4. KALMAN FILTER

4.1. Fundamentals

The KF is a set of mathematical equations which minimizes the root mean square error of the states, related to the measured and the predicted output of a linear system. The advantage of this filter is the prediction of the past, actual and future states of a system even if the dynamic of the system is not well known [3]. The following KF equations are adapted to the battery model of chapter 3.

The filter predicts the states $\underline{x}(t) \in R^n$ of the system with the linear equation

$$\underline{\dot{x}}(t) = \mathrm{A} \cdot \underline{x}(t) + \underline{b} \cdot u(t) + \underline{v}(t) \quad (10)$$

if the measurement equation

$$y(t) = \mathrm{H} \cdot \underline{x}(t) + n \quad (11)$$

with the measurement matrix $\mathrm{H} \in R^{m \times n}$ exists. The matrix $\mathrm{A} \in R^{n \times n}$ represents the dynamic matrix and $\mathrm{B} \in R^n$ the input vector. The variables $\underline{v}$ and $\underline{n}$ represent an independent, zero–mean,

Gaussian process and measurement noise. The process noise matrix Q is related to the process-noise vector and is defined as

$$Q = E\left[\underline{v}\,\underline{v}^T\right] \tag{12}$$

The square measurement noise r is accorded to

$$r = n^2 \tag{13}$$

To design a discrete Kalman filter, the preceding equations must be discretised. To consider the calculation sample time T_s, the fundamental matrix Φ is necessary [3]. Accorded to

$$\Phi(t) = \mathrm{L}^{-1}[(s \cdot \mathrm{I} - \mathrm{A})^{-1}] \tag{14}$$

The fundamental matrix is given by the inverse Laplace transformation of the identity matrix I and the dynamic matrix A. Thereby, the actual state is now describable according to any previous state value $x(t) = \Phi(\mathrm{t} - \mathrm{t_x}) \cdot x(t_x)$.

The discrete fundamental matrix is therefore given by

$$\Phi_\mathrm{k} = \Phi(t_k - t_{k-1}) = \Phi(\mathrm{T_s}) \tag{15}$$

With this transformation, the equations (11) and (12) can be described as

$$\underline{x}_k = \Phi_\mathrm{k} \cdot \underline{x}_{k-1} + \underline{b}_k \cdot u_{k-1} + \underline{v}_{k-1} \tag{16}$$

and the measurement equation yields in

$$y_k = \mathrm{H} \cdot \underline{x}_k + \underline{d} \cdot u_k + n_k \tag{17}$$

The discrete process noise matrix $\mathrm{Q_k}$ can be found in the continuous process-noise matrix Q(t) and the fundamental matrix according to

$$\mathrm{Q_k} = \int_0^{T_s} \Phi(\mathrm{t}) \cdot \mathrm{Q(t)} \cdot \Phi(\mathrm{t})^\mathrm{T} dt \tag{18}$$

If u_{k-1} is constant between sampling instants, the discrete $\underline{\mathrm{b}}_\mathrm{k}$ is obtained from

$$\underline{b}_\mathrm{k} = \int_0^{T_s} \Phi(\mathrm{t}) \cdot \underline{b}(\mathrm{t}) dt \tag{19}$$

The aim of the filter is to calculate the weighted difference between the real measured output y_k and the predicted value from the measurement equation $\hat{y}_k$:

$$\tilde{y}_k = y_k - \hat{y}_k \tag{20}$$

Based on the discrete measurement equation (17) and the state equation (16), this measurement difference yields in

$$\tilde{y}_k = y_k - \mathrm{H}\left(\Phi_\mathrm{k} \cdot \underline{x}_{k-1} + \underline{\mathrm{b}}_\mathrm{k} \cdot u_{k-1}\right) \tag{21}$$

The resultant Kalman filtering equation becomes

$$\underline{\hat{x}}_k = \Phi_\mathrm{k} \cdot \underline{\hat{x}}_{k-1} + \underline{\mathrm{b}}_\mathrm{k} \cdot u_{k-1} + \mathrm{K_k}(\tilde{y}_k) \tag{22}$$

where the first term $\underline{\hat{x}}_k^- = (\Phi_k \cdot \underline{\hat{x}}_{k-1} + \underline{\mathrm{b}}_\mathrm{k} \cdot u_{k-1})$ describes the filter prediction and the second term $\mathrm{K_k}(\tilde{y}_k)$ the correction.

With the a priori estimation $\underline{\hat{x}}_k^- \epsilon\, R^n$ and the a posteriori estimation $\underline{\hat{x}}_k \epsilon\, R^n$ of the same time step k, the estimation error is defined as

$$\underline{e}_k^- = \underline{x}_k - \underline{\hat{x}}_k^- \tag{23}$$

$$\underline{e}_k = \underline{x}_k - \underline{\hat{x}}_k \tag{24}$$

The error covariance of the estimation errors are

$$\mathrm{P_k^-} = E[\underline{e}_k^- \underline{e}_k^{-T}] \tag{25}$$

$$\mathrm{P_k} = E[\underline{e}_k \underline{e}_k{}^T] \tag{26}$$

The a priori error covariance is now calculated with the fundamental matrix Φ_k and the process noise $\mathrm{Q_k}$:

$$\mathrm{P_k^-} = \Phi_\mathrm{k} \cdot \mathrm{P_{k-1}} \cdot \Phi_\mathrm{k}^\mathrm{T} + \mathrm{Q_k} \tag{27}$$

The Kalman gain $\mathrm{K_k} \epsilon\, R^{n \times m}$ is calculated to

$$\mathrm{K_k} = \mathrm{P_k^-} \cdot \mathrm{H^T}(\mathrm{H} \cdot \mathrm{P_k^-} \cdot \mathrm{H^T} + r)^{-1} \tag{28}$$

The a posteriori error covariance $\mathrm{P_k}$ is updated with the Kalman gain to

$$\mathrm{P_k} = (\mathrm{I} - \mathrm{K_k} \cdot \mathrm{H}) \cdot \mathrm{P_k^{-1}} \tag{29}$$

Figure 7 describes the process of the Kalman filter. The prediction calculates the actual system state and the correction adjusts the estimation due to the measured values.

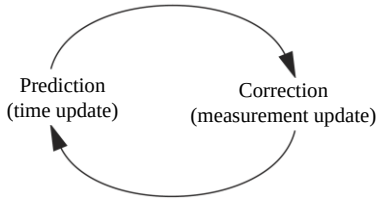

Figure 7: Process of the Kalman filter

This filter structure results in a non-recursive estimation. The new state $\underline{\hat{x}}_k$ is calculated in one single step. For this reason, the calculation performance of this filter is not dependent on the calculation sample time T_s.

4.2. Dual Estimation Structure

In addition to the state of charge (SOC) of a battery system, the state of health (SOH) also has to be estimated. For this purpose, a second KF can be used for estimating the parameters of the cell. Based on the fact, that the space vector form is only given for the state estimation, the prediction part of the parameter KF yields in

$$\underline{w}_k^- = \underline{w}_{k-1} + \underline{s}_{w_{k-1}} \tag{30}$$

where $\underline{s}_{w_{k-1}}$ describes the process noise of the parameter filter [4] and the vector $\underline{w}(t)$ contains the parameter:

$$\underline{w}_k = [w_1, w_2, w_3, w_4]^T = \left[R_{DC,1s_k}, C_{N_k}, R_{D_k}, C_{D_k}\right]^T \tag{31}$$

The resulting parameter process noise matrix S is given by

$$\mathrm{S_k} = E[\underline{s}_{w_k}\, \underline{s}_{w_k}^T] \tag{32}$$

The Kalman equation for the parameter estimation is now set to

$$\hat{w}_k = \hat{w}_k^- + \mathrm{K_{w_k}}(\tilde{y}_k) \tag{33}$$

The difference voltage $\tilde{y}_k$ is the same difference as for the state estimation in equation (21). The adaption of the parameters is therefore only possible by the correction part with the Kalman parameter gain and the difference voltage. To calculate this parameter Kalman gain the equations (27) (28) (29) has to be adapted to the parameter equations (30) (33):

By the reason, that there is no prediction information possible, the fundamental matrix yields in an identity matrix. The a priori error covariance matrix is now updated with the parameter process noise as

$$\mathrm{P_{w_k}^-} = \mathrm{P_{w_{k-1}}} + \mathrm{S_k} \tag{34}$$

Referred to equation (11) the measurement equation for the parameter estimation is now set to

$$y_k = h\left(\underline{x}_k, \underline{w}_k\right) + \underline{n}_k \tag{35}$$

For the Kalman gain calculation the measurement matrix H has to be linearized with the Jacobi matrix $\mathrm{H_w}$ to

$$\mathrm{H_w} = \frac{\partial \mathrm{h}\left(\underline{x}_k, \underline{w}_k\right)}{\partial \underline{\mathrm{w}}_\mathrm{k}} \tag{36}$$

The Kalman gain $K_{w\,k} \epsilon R^{n\times m}$ for the parameter estimator is now calculated to

$$\mathrm{K_{wk}} = \mathrm{P_{wk}^{-}} \cdot \mathrm{H_w^T}\left(\mathrm{H_w} \cdot \mathrm{P_{wk}^{-}} \cdot \mathrm{H_w^T} + r\right)^{-1} \tag{37}$$

The a posteriori error covariance $\mathrm{P_{wk}^{-}}$ is updated with the calculated Kalman gain [5] and the Jacobi Matrix to

$$\mathrm{P_{wk}} = \left(\mathrm{I} - \mathrm{K_{wk}} \cdot \mathrm{H_w}\right)\mathrm{P_{kw}^{-1}} \tag{38}$$

Equations (16) and (30) allow the reference of $h(\underline{x}_k, \underline{w}_k)$ to the previous time step *k-1*. The Jacobi Matrix has therefore not to be derived partially and is given by

$$\mathrm{H_w} = \frac{\partial \mathrm{h}\left(\underline{\hat{\mathrm{w}}}_{\mathrm{k-1}}, \underline{\hat{\mathrm{x}}}_{\mathrm{k-1}}, \underline{\mathrm{u}}_{\mathrm{k-1}}\right)}{\partial \underline{\mathrm{w}}_{\mathrm{k-1}}} \tag{39}$$

This resulting DKF structure is presented in Figure 8

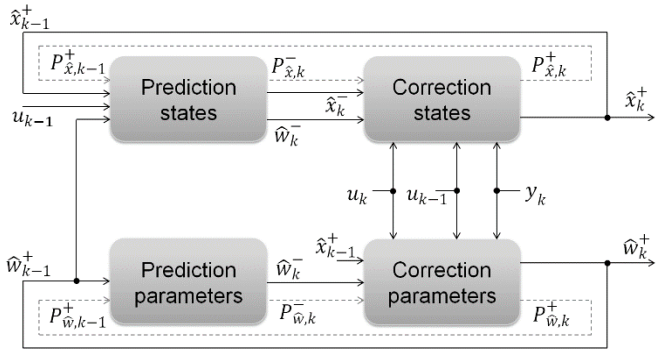

Figure 8: Dual estimation filter structure

Figure 8 shows that both filters have the same input values at the timestamp *k-1* and simultaneously calculate the new values at the timestamp *k*. The combination of both these filters is done at the beginning of each cycle and differs from the common dual parameter estimator [6].

4.3. Implementation

In this section, the battery model of chapter 3 and the KF equations of section 4.1 and 4.2 will be combined for an implementation in the modular BMS of chapter 2.

Recorded to the model equation (8), the fundamental matrix for the battery model is given by

$$\Phi(\mathrm{t}) = \begin{bmatrix} e^{-\frac{t}{R_D \cdot C_D}} & 0 \\ 0 & 1 \end{bmatrix} \xrightarrow[\Phi_\mathrm{K} = \Phi(T_s)]{} \Phi_\mathrm{K} = \begin{bmatrix} e^{-\frac{T_s}{R_D \cdot C_D}} & 0 \\ 0 & 1 \end{bmatrix} \tag{40}$$

According to equation (7) the input value consists of the terminal current I_{KI}. Referred to chapter 2 the current can be calculated in two different ways, the 1 s mean current and the interpolated current. Because the second state is based on the current integration, it will increase the estimation accuracy, if for the second state the averaged current is used instead of the interpolated current. Hence the input vector is given as

$$\underline{u}_{k-1} = \begin{bmatrix} I_{int,k-1} \\ I_{mean,k-1} \end{bmatrix} \tag{41}$$

Recorded to equation (19), $\underline{\mathrm{b}}_\mathrm{k}$ is set to

$$\underline{\mathrm{b}}_\mathrm{k} = \begin{bmatrix} R_D\left(1 - e^{-\frac{T_s}{R_D \cdot C_D}}\right) \\ \frac{T_s}{C_N} \end{bmatrix} \tag{42}$$

The resulted state equation results in

$$\underline{x}_k = \Phi_\mathrm{K} \cdot \underline{x}_{k-1} + \underline{\mathrm{b}}_\mathrm{k} \cdot \underline{u}_{k-1} + \underline{v}_k \tag{43}$$

Referred to equation (18), the process noise matrix Q(t) is set to

$$\mathrm{Q(t)} = \Phi_o \begin{bmatrix} 1 & 0 \\ 0 & 1 \end{bmatrix} \tag{44}$$

A white noise with the spectral density Φ_o adds to both states independently.

The resulted discrete process noise is set to

$$\mathrm{Q_k} = \Phi_o \begin{bmatrix} \frac{R_D \cdot C_D\left(1 - e^{-\frac{T_s}{R_D \cdot C_D}}\right)}{2} & 0 \\ 0 & T_s \end{bmatrix} \tag{45}$$

For the measurement equation, the OCV dependency of the SOC-state will to be normed to the SOC state. The resulting measurement filter equation is described to

$$\hat{y}_k = \mathrm{H_w} \cdot \underline{\hat{x}}_k + \mathrm{D_k} \cdot \underline{u}_k = \begin{bmatrix} 1 \\ \frac{OCV\left(\hat{x}_{2_k}\right)}{\hat{x}_{2_k}} \end{bmatrix} \underline{\hat{x}}_k + \begin{bmatrix} R_{DC,1s_k} \\ 0 \end{bmatrix} \underline{u}_k \tag{46}$$

When the OCV is deposited as a look-up table based on the SOC dependency, this nonlinearity seems like a known and describable correlation to the SOC state. An important issue for the implementation of the filter is the difference between the measurement vectors $y_k - \hat{y}_k$. It is necessary that the equation is referred to the states $\underline{\hat{x}}_{k-1}$ in order to the known vector $\underline{u}_k$. The measurement vector is referred to the actual time step k. Therefore, the equation $\hat{y}_k$ consists of three different current-input values. One is an interpolated current from the previous time step $I_{int_{k-1}}$, the other one is the averaged current from the previous time step $I_{mean_{k-1}}$ and the last one is the actual interpolated current I_{int_k}. The final measurement equation is given by

$$\hat{y}_k = \mathrm{H_w} \cdot \Phi_\mathrm{k} \cdot \underline{\hat{x}}_{k-1} + \mathrm{H_w} \cdot \underline{\mathrm{b}}_\mathrm{k} \cdot \underline{u}_{k-1} + \underline{d}_k \cdot \underline{u}_k \tag{47}$$

with

$$\underline{d}_k = \begin{bmatrix} R_{DC,1s_k} \\ 0 \end{bmatrix} \tag{48}$$

4.4. Optimization

The estimation accuracy of the DKF depends on four criteria: The measurement sample time, the sensor accuracy, the initial values and the adjustment of the processes and measurement noises. Based on the measurement equation (11), the voltage measurement inaccuracy are contained in the measurement noise. Due to the fact, that the current measurement results in an input vector u_k, this inaccuracy is described in the process noise of the equation (10). Referred to the Kalman equations (27) (28) (29), an increasing of the measurement errors r decreases the Kalman gain and reduces the filter performance. An increase in the process noise add up to a more uncertain battery model. The minimization of the squared state error will be approached to the chosen process noise. This results in a more stable filter, but also causes a lower theoretical accuracy.

A wrong value initialization is responsible for a slower convergence of the filter. Therefore, the procedure in the filter optimization contains the following steps:

1. Minimizing the measurement noise, based on the output measurement accuracy

2. Choosing the lowest possible process noise value, whereby the estimation is still converging

The process noise creation of the parameter estimation in particular requires an accurate analysis. Referred to equation (34), the estimated parameter covariance at each cycle is increased by the parameter process noise. Referred to [3], there are three different options to describe this parameter process noise:

1. Constant factor: $\mathrm{S_k} = const.$ That effects a consecutive excitation of the covariance. Thereby the system tends to

diverge but the parameter estimation is dynamic over the cycles.

2. Converge to zero: $S_k = \frac{S_{k-1}}{1+\alpha*k}, \alpha \in [0,1]$ The process noise will be converge to zero, the system becomes more stable. Parameter changes at higher cycle rates will be detected slowly.

3. Forgetting factor: $S_k = P_{w_{k-1}}(1 - \frac{1}{\lambda_{RLS}}), \lambda_{RLS} \in [0..1]$ The process noise is dependent on the previous covariance. It provides an exponentially decaying weighting on past data.

In a BMS for a BEV, only the first option is usable. The second would affect a progressive estimation error, the third option would diverge at less dynamic processes, like the charging or the load free states. Finding the parameter process noise value, which excites the parameter system correctly for a precise estimation and avoids the divagation of the system, is the main goal of the optimization process.

5. BEHAVIOUR OF STATE AND PARAMETER ESTIMATION

For the simulation in a real environment, a li-ion cell (see Table 2) was forced with the Artemis driving cycle.

Table 2: Specifications of the li-ion cell

Name	Panasonic NCR18650PD
Rated capacity	2.68 Ah
End of charge voltage	4.2 V
End of discharge voltage	2.5 V
Max discharge current	10 A
Max charge current	0.825 A

To conform the cycles the battery testing system BaSyTec (see Table 3) was used.
In order to show the behaviour also in the less dynamic charging and load-free states, the driving cycle was expanded to three consecutive cycles:
1. Charge to 93.5 % (4.1 V)
2. Discharge with the Artemis cycle to 11.5 % (3.36 V)
3. Charge to 74 % (3.9 V)
4. Discharge with the Artemis cycle to 11.5 % (3.36V)
   - Charge to 93.5 % (4.1 V)
   - Discharge with the Artemis cycle to 11.5 % (3.36V)
5. Charge to 74 % (3.9 V)

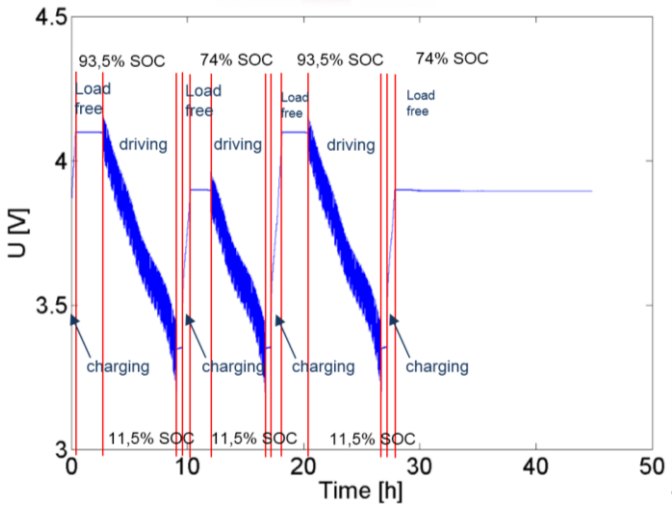

Figure 9: Cycle description

Table 3: Specifications of the BaSyTec testing system

Voltage resolution	±0.25 mV
Current resolution	±0.25 mA
Voltage accuracy	±0.05 %
Current accuracy	±0.1 %

5.1. State Estimation

Figure 10 illustrates the estimated SOC of the DKF, based on the inaccurate current sensor (Table 1 B). In order to evaluate the behaviour of the filter, the proper ampere hour counting is also plotted.

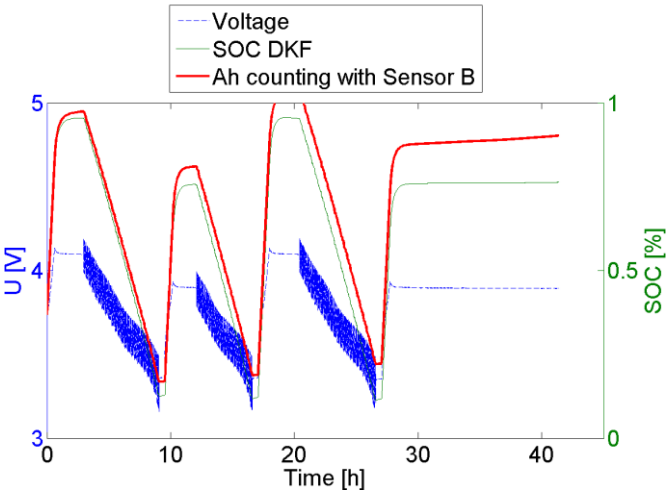

Figure 10: Estimated SOC compared with ampere hour counting (sensor B)

The DKF adapts to the demand cycle reference points at the end of each driving and charging cycle. The DKF shows a smooth estimation behaviour, relating to the inaccurate current sensor. The ampere hour counting diverges as anticipated due to the inaccurate measurement. Figure 11 presents the covariance of the filter. As already observed at the SOC estimation, the covariance demonstrates an accurate working behaviour, based on the DKF. In the dynamic period the covariance decrease, whereas increases in the less dynamic charging period.

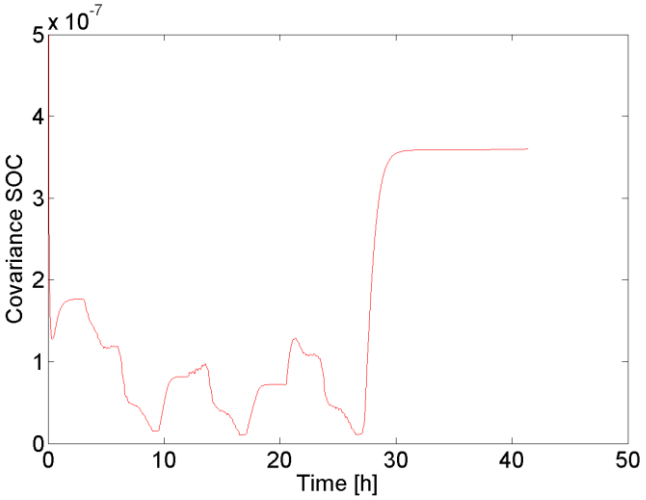

Figure 11: Covariance of the SOC

Figure 12 now shows the state estimation behaviour of the filter with the more accurate current sensor A (Table 1 A). The improvements by the KF are marginal whereby the independence of the current sensor used in the state estimation is demonstrated.

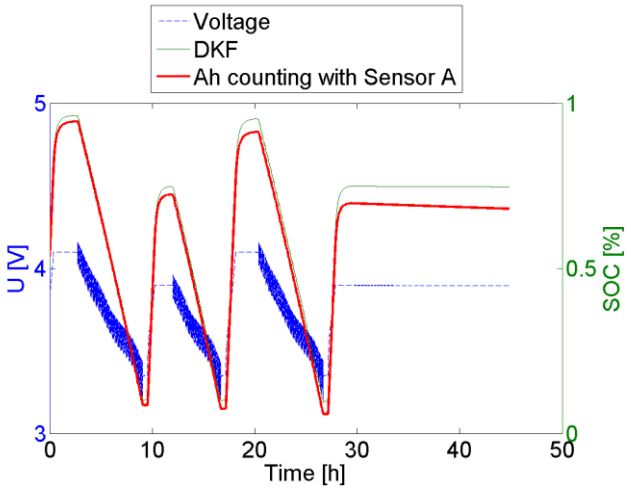

Figure 12: Calculated SOC with sensor A

5.2. Parameter Estimation

Because the parameter equation depends only on the measurement vector, as shown in equation (30), a precise estimation needs a high excitation of the battery system, otherwise the correction part in the parameter estimation (equation (33)) will not adapt to the proper parameter. Figure 13 shows the estimation of the $R_{DC,1s}$resistor and the proper covariance (Figure 14) with the accurate sensor. As expected, the covariance increases in areas of less dynamic curve segments, like the constant voltage charging or the load-free mode. When there is an excitation process, based on the Artemis driving cycle, the estimated parameter converges fast to the proper value. Related to equation (5), the $R_{DC,1s}$resistor equation is based on the current measurement. Therefore, the estimated $R_{DC,1s}$ resistor depends on the accuracy of the current sensor used. Figure 15 shows the estimated resistor, based on the estimated SOC. It shows a typical behaviour, especially at the end of the discharging process, the resistor increases and will causes a power decrease of the cell.

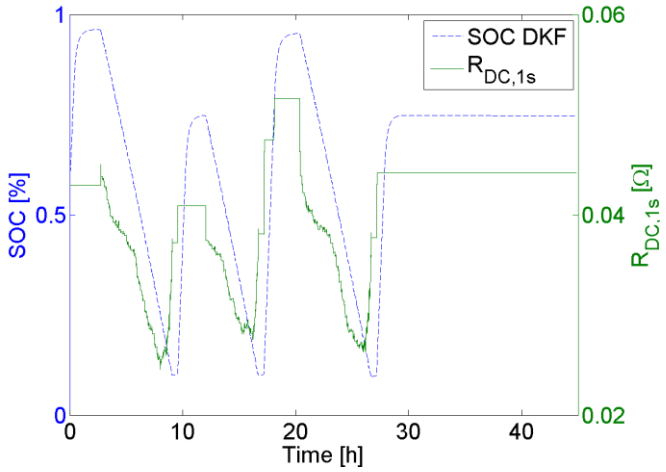

Figure 13: Estimated $R_{DC,1s}$resistor with sensor A

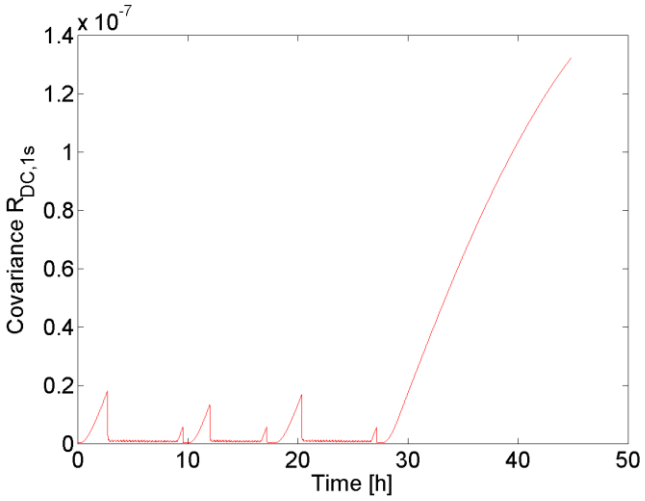

Figure 14: Covariance of the $R_{DC,1s}$resistor with sensor A

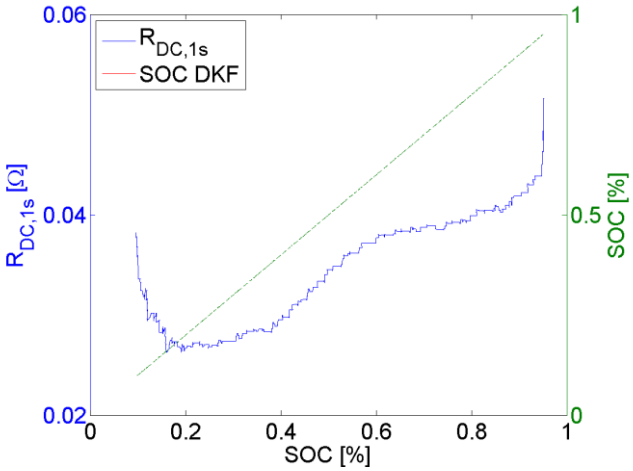

Figure 15: Estimated $R_{DC,1s}$cell resistant, referred to the SOC

The two parameters R_D and C_D influence the dynamic behaviour of the battery model. Figure 16 shows the diffusion time constant related to six driving charging cycles. The time constant changes significantly over the cycles. The filter corrects the initialized time constant of 30 s to a value around 90 s and shows therefore a slow convergence behaviour at not exact initial values. It takes more driving charging cycles until the accorded value is reached. The cell capacity C_N and the diffusion capacity C_D change slowly. Therefore a correct value initialization, especially for those two capacity parameters is essential for an accurate parameter estimation. The convergence of those values by an inaccurate initialization could take an indefinite time or in the worst case it will cause a diverging behaviour. Based on this initialization issue, the estimated parameters must be latched for an after and after proper initialization. This can be done on the BMS or offline on a server platform. This data are essential for a reliable working BMS.

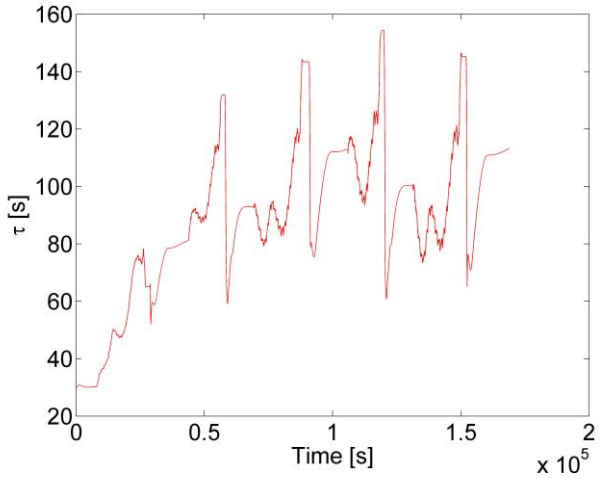

Figure 16: Estimated diffusion time constant related to sensor A

5.3. Processing power

The calculation time for one battery cell, based on the implemented KF with the presented battery model reveals 200000 cycles. Accorded to the BMS structure in Figure 2, based on the used processing unit, this BMS can theoretically estimate the states and parameters of more than 625 cells per second. In practice the estimation performance will decreased due to the other BMS functions. Regarded to the modular extension possibility of the modular BMS, the calculation sample time Ts depends on the number of used cells. When the sample time Ts has to be 100 ms instead of 1 s, the theoretically usable cell number decreases to less than 62. The processing power of the slaves would not be enough for the full modular extension capability of 72 cells per module (referred to chapter 1). Figure 17 demonstrates the different calculated SOC states at different sampling times (1 s and 100 ms). An improvement of the KF estimated SOC output based on a much lower sampling time is not observable. This issue is based on the fact that the KF does not need to be linearized and consequently the calculations performance does not depend on the sampling calculation time.

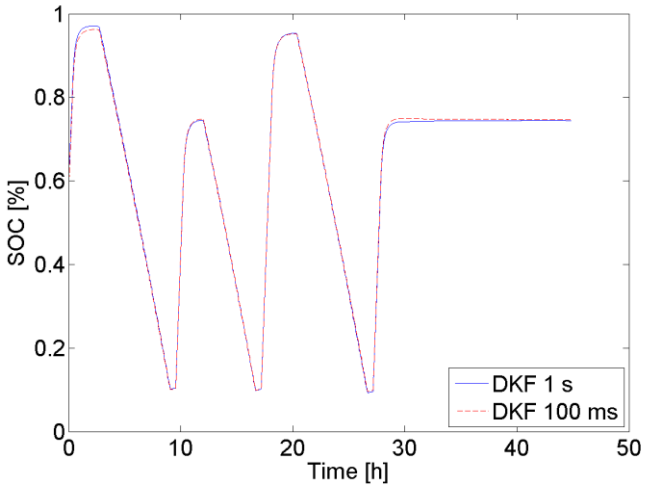

Figure 17: Filter behaviour compared to 1 s and 100 ms calculation sample time

6. VERIFICATION

6.1. Verification of the SOC Estimation

To verify the calculated SOC, a new cycle was provided. The new cycle consist of the first four steps of the driving cycle described in chapter 5, in which the second Artemis cycle is interrupted at 3.7 V. Then, after a 3 h rest time, the cell was fully discharged with a constant current to the end of discharge voltage of 2.5 V followed with a constant voltage discharge to a current of 0.134 A (Figure 18). With the ampere hour counter of the BaSyTec a removed capacity of $C_R = 1.765\,Ah$ was measured. With the previous measured usable capacity of $C_N = 2.759\,Ah$ the SOC_{AhC} is calculated as follows:

$$SOC_{AhC} = \frac{C_R}{C_N} = \frac{1.765\,Ah}{2.759\,Ah} = 0.6397 \rightarrow 63.97\,\% \quad (49)$$

This capacity is compared to the estimatedSOC_{DKF}:

$$\Delta SOC = SOC_{DKF} - SOC_{AhC} = 64.21 - 63.97 = 0.24\,\% \quad (50)$$

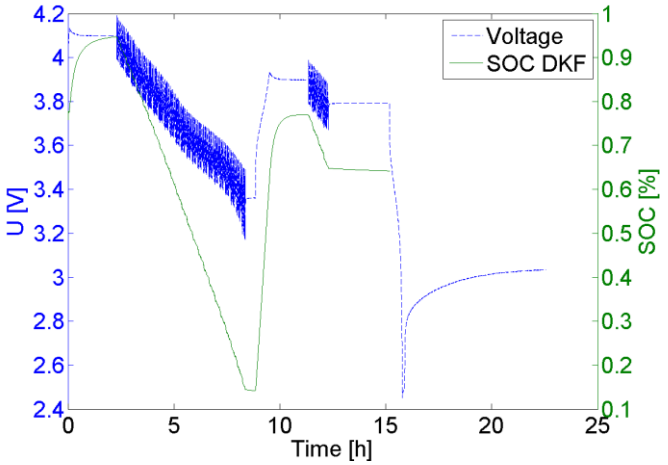

Figure 18: Test procedure for the SOC verification

This verification was executed with the more inaccurate current sensor B (Table 1). However, the SOC algorithm reveals a high accuracy and an independency of the current sensor used accuracy. The SOC estimation refer the state calculation more to the OCV dependency then to the current integration. An inaccurate OCV curve would decrease the state estimation significantly and therefore an accurate OCV determination is necessary for a reliable state estimation.

7. CONCLUSION AND OUTLOOK

In the presented work the behaviour of a dual Kalman filter, implemented on a modular BMS has been described. Based on the calculation structure of a discrete Kalman filter, a Kalman Filter was adapted to the proper battery model. This Kalman filter yielded in an accurate state estimation at a low processing power. The paper revealed that for an implementation of such a filter, several implementation processes have to be considered. Differences in the sampling rate and in the measurement accuracy affect the performance of the algorithm. Several optimization issues were shown and the importance of the process and measurement noise adjustment was explained. The correlation between the measured values and the achieved estimations were revealed. Moreover, the problems in the parameter estimation, based on dynamic loads were discussed and their impacts on the estimated values were presented.

The KF provides a reliable performance in an accurate SOC estimation, within an error less than 0.24 %. The dependency on the current sensor used and the importance of a correct filter initialization must be considered for the BMS architecture. Improvements of several BMS functions such as the cell balancing, the charging time or the energy management can be modelled with this algorithm. To rely on the estimated battery states, much more critical scenarios have to be analysed. The filter behaviour with respect to the battery lifetime and the filter performance in failure scenarios has to be investigated as well.

The parameter estimation shows differences in the estimation accuracy, depending on the actual loads. Uncertainty at the initialization process could result in inaccurate parameter estimations. Referred to the state estimation, the parameter estimation needs further investigations of the BMS measurement accuracy and of the optimization processes. The KF shows an improvement in the calculation complexity with a cycle count of 82k cycles for one cell. The resultant behaviour shows that a reliable parameter estimation is only possible in high dynamic procedures. For an efficient power prediction or an accurate temperature management, additional parameter equations are necessary to improve the prediction procedure. The verification of the estimated cell capacity was hardly possible, based on the slowly changing behaviour of the capacity parameters and would require long cycle investigations.

8. ACKNOWLEDGMENTS

Acknowledgements go to all associates and supporting companies. The use of facilities at the EES (Inst. for Electrical Energy Storage Technology) and FTM (Inst. of Automotive Technology) and enlightening discussions with Martin Brand are gratefully acknowledged. The author would also like to thank the reviewers for their corrections and helpful suggestions. The project was conducted with basic research funds of FTM and EES.

9. REFERENCES

[1] C. Linse, M. Brand, J. Dambrowski, and A. Jossen, "Model-based parameter estimation of li-ion batteries," *Kraftwerk Batterie*, 2012.

[2] G. L. Plett, "High-performance battery-pack power estimation using a dynamic cell model," *IEEE Transactions on Vehicular Technology*, vol. 53, pp. 1586–1593, 2004.

[3] P. Zarchan and H. Musoff, *Fundamentals of Kalman Filtering*. AIAA, 2009.

[4] E. A. Wan and R. van der Merwe, *Kalman Filtering and Neural Networks*. John Wiley & Sons, 2001, ch. The Unscented Kalman Filter, pp. 221–280.

[5] G. L. Plett, "Extended Kalman filtering for battery management systems of liPB-based HEV battery packs - part 1. background," *Journal of Power Sources*, vol. 134, pp. 252–261, 2004.

[6] E. A. Wan and A. T. Nelson, *Kalman Filtering and Neural Networks*. John Wiley & Sons, 2001, ch. Dual Extended Kalman Filter Methods, pp. 123–173.